RESEARCH ARTICLE

Improved Thermal Stability of Dielectric and Electrical Properties of Chemically Modified $Na_{0.5}Bi_{0.5}TiO_3$ Based Ceramics

Aamir Jalil[1], Shah Faisal[2], Abdul Manan[1,*], Imran Ullah[1], Safeer Ahmad[3] and Ameer Ullah[1]

[1] Laboratory for Research in Advanced Materials, Department of Physics, University of Science & Technology Bannu, Bannu 28100, Pakistan
[2] Department of Chemical Sciences, University of Science & Technology Bannu, Bannu 28100, Pakistan
[3] Center for Materials Science, Islamia College Peshawar, Peshawar 25120, Pakistan

Abstract

In the present study, $Na_{0.329}Bi_{0.329}Ba_{0.042}Sr_{0.30}TiO_3$ (NBBST) and its solid solutions with $Nd(Mg_{0.5}Ti_{0.5})O_3$ (NMT), $Nd(Mg_{2/3}Nb_{1/3})O_3$ (NMN), and $Nd(Zn_{2/3}Nb_{1/3})O_3$ (NZN) were synthesized and investigated. The phase composition, microstructure, dielectric properties, and impedance characteristics were analyzed for their optimized dense sintered forms. X-ray diffraction (XRD) confirmed the formation of a single-phase perovskite structure in all compositions within the detection limit. All ceramics exhibited dense microstructures; however, the doped samples showed a reduced average grain size compared to pure NBBST. Among the compositions studied, the 0.98NBBST-0.02NZN solid solution demonstrated superior dielectric and electrical performance. This composition exhibited a low electrical conductivity ($\sim 3.98 \times 10^{-7}\,\mathrm{S/cm}$ at $600\,^{\circ}\mathrm{C}$ and at a frequency of $100\,\mathrm{Hz}$), low dielectric loss ($\tan\delta < 0.05$), and a high dielectric constant ($\varepsilon_r \approx 2500$), with excellent temperature stability of capacitance from below room temperature up to $324\,^{\circ}\mathrm{C}$. Additionally, the Cole-Cole plot of the 0.98NBBST-0.02NZN ceramic revealed a higher resistance at $600\,^{\circ}\mathrm{C}$ compared to the other investigated compositions.

Keywords: dielectrics, impedance spectroscopy, electrical conductivity.

1 Introduction

Researchers have been actively investigating ferroelectric perovskite-based materials since the 1940s due to their versatile functional properties [1]. In recent years, interest in these materials has intensified, particularly in the context of power electronic applications such as electric vehicles, wind turbine generators, underground gas and oil exploration, and advanced propulsion systems. These technologies often involve environments where temperatures

Submitted: 24 May 2026
Accepted: 29 June 2026
Published: 10 July 2026

Vol. 2, **No.** 3, 2026.
10.62762/JAEM.2026.170619

***Corresponding author:**
✉ Abdul Manan
drmanan82@yahoo.com, drmanan82@ustb.edu.pk, arbab.safeer@icp.edu.pk

Citation
Jalil, A., Faisal, S., Manan, A., Ullah, I., Ahmad, S., & Ullah, A. (2026). Improved Thermal Stability of Dielectric and Electrical Properties of Chemically Modified $Na_{0.5}Bi_{0.5}TiO_3$ Based Ceramics. *Journal of Advanced Electronic Materials*, 2(3), 69–81.

exceed 150 °C [2, 3], creating a pressing need for ceramic capacitors capable of stable operation within a wide temperature range of 200–300 °C [3–5]. Extensive research has demonstrated this requirement across a range of perovskite-based dielectric systems [6–10].

To standardize capacitor performance across varying temperatures, the Electronic Industries Association (EIA) classifies materials by their temperature coefficient of capacitance (TCC) using codes such as X7R, X8R, X9R, and Y9R. Here, "X" and "Y" refer to minimum operating temperatures of −55 °C and −30 °C, respectively, while the digits "7," "8," and "9" represent maximum operating temperatures of 125 °C, 150 °C, and 200 °C. The "R" indicates a capacitance variation within ±15% across the specified range [11]. Achieving such thermal stability, particularly at elevated temperatures, is a key goal in the development of advanced dielectric materials.

Relaxor ferroelectrics—materials with diffuse phase transitions and polar nanoregions (PNRs)—are promising candidates for high-temperature capacitor applications due to their superior dielectric stability. Previous studies have demonstrated that compositional engineering via multiple ion substitutions at the A- and B-sites of the ABO_3 perovskite lattice is an effective strategy for tailoring the dielectric response of relaxor ferroelectrics. Substitutions at the A-site—such as partial replacement of Bi or Na by other cations—modify the local polar order and shift the depolarization temperature, thereby altering the phase evolution and broadening the ε_r–T profile [12, 20]. Simultaneous B-site modifications, including the introduction of complex oxides such as $Bi(Zn_{0.5}Ti_{0.5})O_3$ or $BiScO_3$, promote relaxor behavior by disrupting the long-range ferroelectric order and fostering the formation of polar nanoregions (PNRs), which suppress the sharp Curie-type peak [14, 22]. The role of PNRs in producing a flattened ε_r–T response has been corroborated by nanoscale structural studies [22]. Furthermore, the incorporation of $NaNbO_3$ as a modifier in NBT-based systems has proven particularly effective in stabilizing the dielectric constant over a broad temperature range [17, 18]. Through these strategies, capacitance variation within ±15% has been achieved over temperature windows exceeding 200 °C in several systems: for example, from −20 °C to 430 °C in $BaTiO_3$–$Bi(Mg_{0.5}Zr_{0.5})O_3$ [16], from −60 °C to 300 °C in related NBT-based ceramics [15], and over comparably wide windows in BCT–BZT and BCT–BZT–$NaNbO_3$ compositions [13]. In addition, A-site deficiency and aliovalent co-substitution at both sites have been shown to generate anomalously high dielectric constants alongside improved temperature stability [23, 24]. The relaxor behavior induced by such substitutions also promotes low remnant polarization and slim hysteresis loops, which are simultaneously beneficial for high energy storage density applications [19, 21]. These materials are known as temperature-stable relaxors.

Temperature-stable relaxors can be grouped based on their dielectric constant and operational range. Materials with medium dielectric constant values ($\varepsilon_r \sim$ 1000–1200) can typically withstand upper temperature limits of 300–400 °C; however, their lower limit is often above −55 °C, failing to meet EIA standards. In contrast, materials with modest ε_r ($\sim$ 450–500) can satisfy the full target range from −55 °C to 300 °C but may compromise on volumetric efficiency due to their lower dielectric constant. Moreover, several reported systems suffer from high dielectric loss, which limits their practical applicability [3].

To address these limitations, recent research has focused on compositional engineering of lead-free perovskites such as $Na_{0.5}Bi_{0.5}TiO_3$ (NBT). NBT has a high Curie temperature ($T_C \sim 320$ °C) [25, 26] and a rhombohedral R3c structure at room temperature [27], making it a suitable base material. However, in its pure form, NBT exhibits a limited working temperature range. Solid solutions of NBT with $BaTiO_3$ (BT), particularly in the morphotropic phase boundary (MPB) region for $x = 0.06$–0.07 in $(1–x)$NBT–xBT, show enhanced piezoelectric responses but with a narrow thermal operating window. Similarly, ternary systems such as NBT–$Bi_{0.5}K_{0.5}TiO_3$–$BiCrO_3$ have been explored to further tune the piezoelectric and dielectric properties, though they also face challenges in achieving broad thermal stability [28].

To broaden the temperature range, various compositional modifications have been introduced. For example, Su et al. [29] reported a composition of $(1-x)(0.94\text{NBT}-0.06\text{BT})-x\text{KTaO}_3$ ($x = 0.30$) that achieves a high ε_r of 1094 at 25 °C and a TCC within ±15% from −70 °C to 200 °C. Similarly, the addition of $SrTiO_3$ in $(1-x)[0.94\text{NBT}-0.06\text{BT}]-x\text{SrTiO}_3$ led to a broadened ε_r-T curve for $x = 0.30$ [30]. Pan et al. [31] demonstrated that $Nd(Mg_{2/3}Nb_{1/3})O_3$ can effectively flatten the ε_r-T response in NBT-based ceramics by promoting relaxor behavior through the development of PNRs. Li et al. [32] further showed that $Nd(Zn_{2/3}Nb_{1/3})O_3$ could suppress

the sharp Curie peak in $BiFeO_3$-$BaTiO_3$ systems. Other rare-earth-based complex perovskites such as $Sm(Mg_{0.5}Ti_{0.5})O_3$ and $Nd(Mg_{0.5}Ti_{0.5})O_3$, which exhibit low dielectric constants (~25–26), have also been employed as chemical modifiers to broaden the ε_r-T characteristics in perovskite systems [33, 35, 36]. These chemical modifiers induced relaxor behavior by disrupting the long-range ferroelectric order and promoted PNRs formation, ultimately leading to improved temperature stability. It is well established that the microstructural characteristics—including grain size, grain boundary density, and defect distribution—play a critical role in determining the dielectric and electrical properties of perovskite ceramics [34].

In the present study, $Nd(Mg_{0.5}TiO_{0.5})O_3$ (NMT), $Nd(Mg_{2/3}Nb_{1/3})O_3$ (NMN), and $Nd(Zn_{2/3}Nb_{1/3})O_3$ (NZN) are employed as chemical modifiers to enhance the relaxor characteristics of $Na_{0.329}Bi_{0.329}Ba_{0.042}Sr_{0.30}TiO_3$ (NBBST). The objective is to develop lead-free, low-loss, and temperature-stable perovskite ceramics with high dielectric constants, suitable for use in high-temperature power electronic applications.

2 Experimental procedure

In the present study, all ceramic compositions were synthesized via the conventional solid-state reaction method. High-purity raw materials were used as starting reagents: Bi_2O_3 (99.9%, Sigma-Aldrich), Na_2CO_3 (99.99%, Sigma-Aldrich), $SrCO_3$ (99.95%, Sigma-Aldrich), $BaCO_3$ (99.99%, Sigma-Aldrich), MgO (99.99%, Sigma-Aldrich), TiO_2 (99+%, Sigma-Aldrich), Nd_2O_3 (99.99%, Sigma-Aldrich), Nb_2O_5 (99.9%, Sigma-Aldrich), and ZnO (99.99%, Sigma-Aldrich). Prior to weighing, all powders were preheated at 200 °C to remove any adsorbed moisture. The compositions prepared included the base $Na_{0.329}Bi_{0.329}Ba_{0.042}Sr_{0.30}TiO_3$ (NBBST) and its solid solutions with 2 mol% of $Nd(Mg_{0.5}Ti_{0.5})O_3$ (NMT), $Nd(Mg_{2/3}Nb_{1/3})O_3$ (NMN), and $Nd(Zn_{2/3}Nb_{1/3})O_3$ (NZN).

The required raw materials were weighed in stoichiometric proportions and thoroughly mixed using ball milling for 24 hours in ethanol to ensure homogeneity. The resulting slurry was dried and the powders were calcined at 800 °C for 2 hours in air. The calcined powders were manually ground using an agate mortar and pestle to obtain fine powders. These were then pressed into cylindrical pellets of 10 mm diameter and approximately 1 mm thickness using a uniaxial hydraulic press (MTI, EQ-HP-88V-LD) at an applied pressure of 100 MPa.

The green pellets were placed on a bed of alumina powder and sintered at 1200 °C for 2 hours in a box-type muffle furnace to achieve dense microstructures. After sintering, both faces of the pellets were polished to obtain smooth surfaces. A portion of the sintered pellets was crushed into powder form and analyzed using X-ray diffraction (XRD, PANalytical) over a 2θ range of 20° to 80° to identify the crystalline phases and verify the formation of the perovskite structure.

To observe the surface morphology, selected sintered samples were thermally etched at 1080 °C for 30 minutes and analyzed using a scanning electron microscope (SEM). For dielectric measurements, the flat surfaces of the polished pellets were coated with silver paste and fired at 550 °C for 1 hour to form conductive electrodes. The dielectric constant (ε_r) and dielectric loss ($\tan\delta$) were measured using an impedance analyzer (Microtest-6632, Taiwan) at frequencies of 1 kHz, 100 kHz, 250 kHz, and 1 MHz across the temperature range of interest.

Further, the real (ε') and imaginary (ε'') parts of the dielectric permittivity were recorded over a frequency range of 100 Hz to 1 MHz at elevated temperatures between 500 °C and 600 °C. Based on these measurements, additional properties such as electrical conductivity (σ), complex impedance (Z), and electric modulus (M) were calculated to assess the electrical behavior of each composition in detail.

3 Results and Discussions

3.1 Phase Analysis

Figure 1 presents the room-temperature X-ray diffraction (XRD) patterns of the NBBST, 0.98NBBST–0.02NMT, 0.98NBBST–0.02NMN, and 0.98NBBST–0.02NZN ceramics. All compositions exhibit similar diffraction patterns, with peaks well matched to the standard JCPDS card no. 46-0001, corresponding to the perovskite phase of NBT-BT ceramics. No secondary or impurity phases were detected within the resolution limit of the XRD, confirming the successful formation of a single-phase perovskite structure in all compositions.

A magnified view of the (200) diffraction peak, located around 46°–47° (2θ), reveals a slight peak shift among the doped samples, indicating subtle changes in the lattice structure due to cationic substitutions. In these

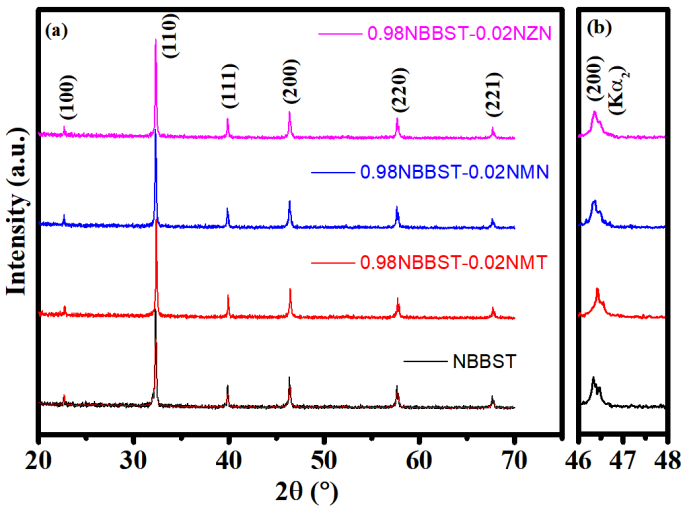

Figure 1. XRD patterns of sintered NBBST, 0.98NBBST-0.02NMT, 0.98NBBST-0.02NMN, and 0.98NBBST-0.02NZN ceramics, confirming the formation of a single-phase perovskite structure.

compositions, substitutions occur simultaneously at both the A-site and B-site of the ABO_3 perovskite structure. The A-site substitutions involve Nd^{3+} ($r = 1.27$ Å), which has a smaller ionic radius than the average A-site ionic radius in the base composition $[(Na_{0.32} + Bi_{0.32} + Ba_{0.04} + Sr_{0.29})^{2+}]$, $r \approx 1.43$ Å. This tends to contract the unit cell. Conversely, B-site substitutions involve larger effective ionic radii:

$$(Mg_{0.5}Ti_{0.5})^{3+} \quad (r \approx 0.66\,\text{Å}),$$
$$(Mg_{2/3}Nb_{1/3})^{3+} \quad (r \approx 0.68\,\text{Å}),$$
$$\text{and } (Zn_{2/3}Nb_{1/3})^{3+} \quad (r \approx 0.69\,\text{Å}),$$

compared to the radius of Ti^{4+} ($r = 0.60$ Å) [37], which would normally promote lattice expansion.

However, the observed peak shifts are toward higher 2θ angles, which suggests an overall contraction of the unit cell. This indicates that the effect of the A-site substitution by smaller Nd^{3+} ions dominates over the slight expansion introduced by the larger B-site substituents. Additionally, no splitting of the (200) peak is observed—apart from the minor contribution from Cu $K_{\alpha 2}$ radiation—implying that the samples retain a pseudo-cubic structure [38, 39].

These results confirm that all substituted cations are effectively incorporated into the host lattice, forming complete solid solutions with the NBBST matrix. The absence of secondary phases and the consistent peak shifts validate the structural integrity and compositional homogeneity of the synthesized ceramics.

3.2 Microstructural study

Figure 2 displays the surface morphologies of thermally etched NBBST, 0.98NBBST–0.02NMT, 0.98NBBST–0.02NMN, and 0.98NBBST–0.02NZN ceramics sintered at 1200 °C. All compositions exhibit dense microstructures with well-defined grain boundaries and minimal visible porosity, indicating effective densification during sintering. The corresponding grain size distribution curves, obtained using ImageJ software, are also provided for each sample.

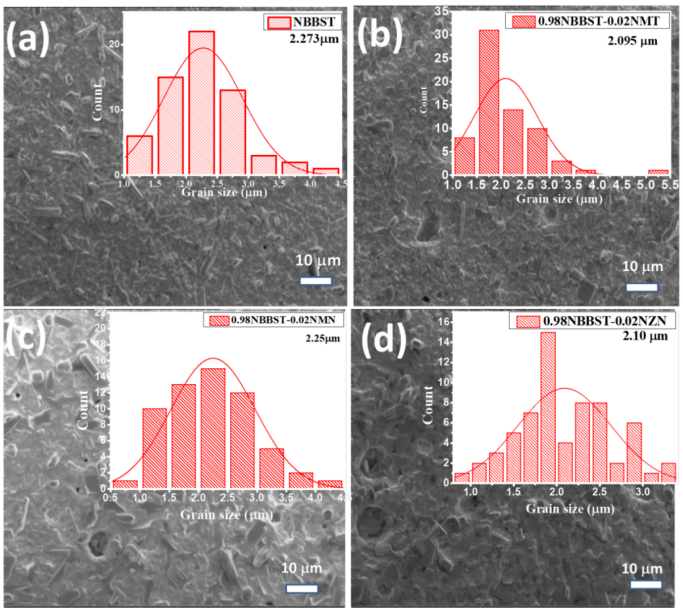

Figure 2. SEM micrographs of (a) NBBST, (b) 0.98NBBST-0.02NMT, (c) 0.98NBBST-0.02NMN, and (d) 0.98NBBST-0.02NZN ceramics, illustrating dense microstructures and grain morphology.

The average grain sizes were found to be 2.27 μm for NBBST, 2.09 μm for 0.98NBBST–0.02NMT, 2.25 μm for 0.98NBBST–0.02NMN, and 2.10 μm for 0.98NBBST–0.02NZN. These results indicate a modest reduction in grain size in the doped samples compared to the undoped NBBST. The grain growth suppression can be attributed to the effect of cationic substitutions at both A- and B-sites, which introduce lattice strain and disrupt the diffusion-driven grain growth process. The finer and more uniform microstructure in the doped samples is beneficial for improving dielectric and electrical properties, particularly in reducing leakage current and enhancing resistivity.

3.3 Dielectric Properties

Figure 3(a–d) shows the dielectric constant (ε_r) and dielectric loss ($\tan\delta$) as a function of temperature for NBBST, 0.98NBBST–0.02NMT, 0.98NBBST–0.02NMN,

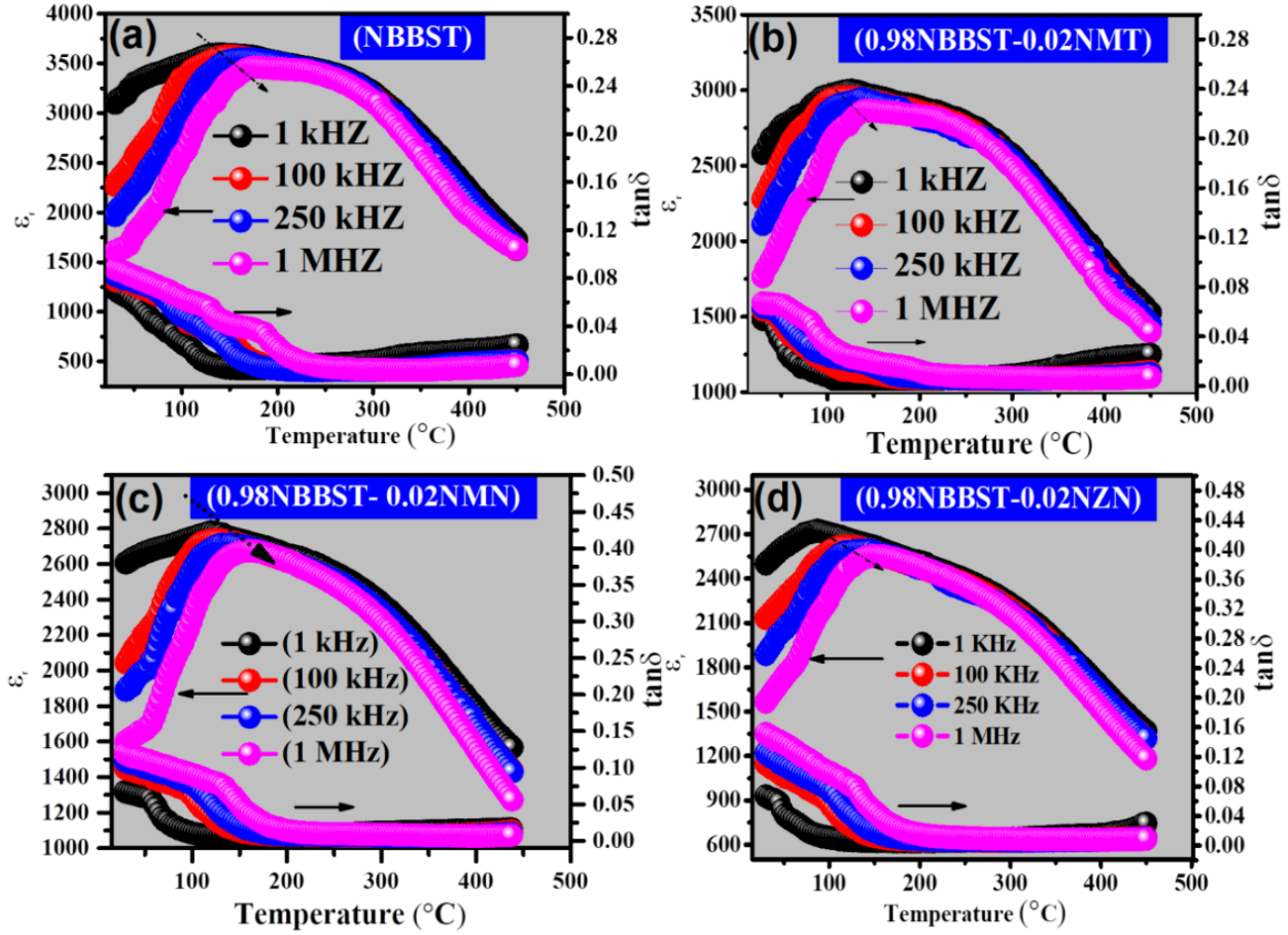

Figure 3. Temperature dependence of dielectric constant (ε_r) and dielectric loss (tanδ) at various frequencies for (a) NBBST, (b) 0.98NBBST-0.02NMT, (c) 0.98NBBST-0.02NMN, and (d) 0.98NBBST-0.02NZN ceramics.

and 0.98NBBST–0.02NZN ceramics, measured in the frequency range of 1 kHz to 1 MHz over a temperature range of 30 °C to 450 °C. For all compositions, the ε_r initially increases with increasing temperature, reaches a broad maximum (forming a plateau), and then decreases at higher temperatures. This behavior is attributed to increased thermal vibrations of the lattice and enhanced phonon–dipole interactions, which reduce the overall dipolar alignment capability at elevated temperatures [40].

A noticeable frequency dispersion is observed in the dielectric constant peaks, *i.e.*, shifts toward higher temperatures occurred with increasing frequency. This is a characteristic signature of relaxor-type ferroelectrics [41, 42]. In such materials, multiple polarization mechanisms—electronic, ionic, dipolar, and space-charge—contribute to the total polarization at low frequencies. However, as the frequency increases, the slower mechanisms (particularly space-charge and dipolar polarization) fail to respond, resulting in a reduced dielectric constant. Among these mechanisms, electronic and ionic polarization respond almost instantaneously at frequencies up to optical range, while dipolar and space-charge polarization are significantly slower and cease to contribute at sufficiently high frequencies [41, 42]. Consequently, the decrease in ε_r with increasing frequency reflects the inability of slower mechanisms to follow the alternating electric field.

Importantly, no distinct dielectric anomaly (commonly referred to as the depolarization temperature, T_d) was observed at low temperatures in any of the compositions, suggesting a transition into a highly frustrated, ergodic relaxor state dominated by polar nanoregions (PNRs) in all investigated compositions [44]. Such relaxor-type compositions with suppressed long-range polar order typically exhibit reduced remnant polarization and slimmer hysteresis loops compared to normal ferroelectrics, which is advantageous for capacitor

applications requiring low dielectric loss and stable charge–discharge behavior [48].

Dielectric losses ($\tan\delta$) are influenced by intrinsic material conductivity and energy dissipation due to atomic, molecular, and electronic vibrations, particularly at high frequencies. Various cation substitutions in NBBST resulted in a downward shift of the Curie peak along with reduced ε_r and $\tan\delta$ values, as shown in Figure 3(d). The maximum dielectric constants (ε_{max}) recorded were approximately 3100 for NBBST, 2581 for 0.98NBBST–0.02NMT, 2606 for 0.98NBBST–0.02NMN, and 2500 for 0.98NBBST–0.02NZN. This reduction in ε_r can be linked to the lower ionic polarizabilities of the substituted cations. In particular, 0.98NBBST–0.02NZN exhibits the lowest ε_r and $\tan\delta$ among all compositions, which is attributed to the lower dielectric polarizabilities of Zn ($2.04\,\text{Å}^3$) and Mg ($1.32\,\text{Å}^3$) compared to Ti ($2.93\,\text{Å}^3$) [43]. These differences in ionic polarizability have similarly been invoked to rationalize dielectric property variations in other lead-free perovskite systems [45, 46].

To evaluate the temperature stability of the ceramics, the normalized capacitance variation for NBBST, 0.98NBBST–0.02NMT, 0.98NBBST–0.02NMN, and 0.98NBBST–0.02NZN ceramics was measured at 1 kHz. The temperature range within which the capacitance variation remains within $\pm15\%$ defines the operating window for stable dielectric performance.

The upper operating temperature limits (i.e., the temperatures at which TCC exceeds $\pm15\%$) were determined to be approximately 123 °C, 105 °C, 333 °C, and 324 °C for NBBST, 0.98NBBST–0.02NMT, 0.98NBBST–0.02NMN, and 0.98NBBST–0.02NZN, respectively, as shown in Figure 4. In all cases, the lower operating limit was found to be below room temperature (RT), indicating stable performance in sub-ambient conditions. These results clearly demonstrate that the introduction of various cationic substitutions at both A- and B-sites of the NBBST perovskite matrix significantly enhances the

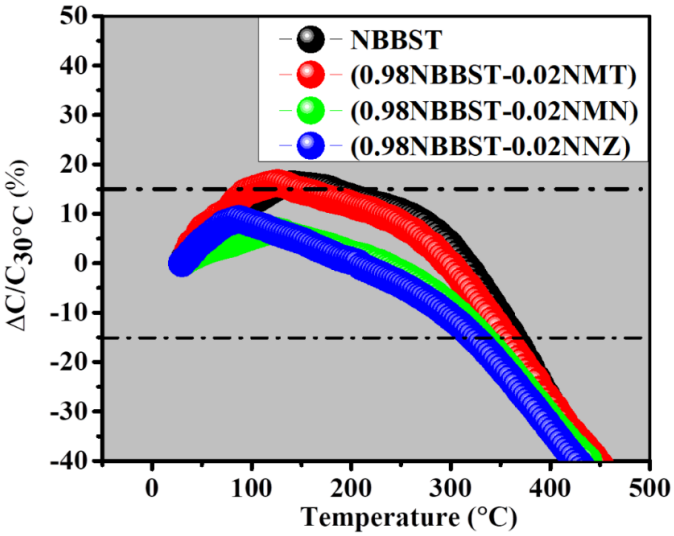

Figure 4. Temperature-dependent variation of normalized capacitance ($\Delta C/C_{30°C}$) measured at 1 kHz for NBBST, 0.98NBBST–0.02NMT, 0.98NBBST–0.02NMN, and 0.98NBBST–0.02NZN ceramics.

temperature stability of capacitance. The broader temperature stability window, especially in the NMN and NZN doped compositions, suggests enhanced relaxor behavior due to the formation of polar nano-regions (PNRs).

Among all compositions, 0.98NBBST–0.02NZN exhibited the widest temperature stability range (<RT to 324 °C) along with a high dielectric constant ($\varepsilon_r > 1800$), surpassing many relaxor-type NBT-based ceramics reported in literature [29, 47, 49]. This makes it a promising candidate for high-temperature capacitor applications, particularly in power electronics. A comparative summary of the temperature coefficient of capacitance (TCC) performance of 0.98NBBST–0.02NZN with other reported NBT-based relaxor materials is provided in Table 1.

Figure 5(a–e) presents the Nyquist (Cole–Cole) plots of $-Z''$ versus Z' for NBBST, 0.98NBBST–0.02NMT, 0.98NBBST–0.02NMN, and 0.98NBBST–0.02NZN ceramics, measured over the temperature range of $500--600\,°C$ in the frequency range of 100 Hz

Table 1. Comparison of the temperature coefficient of capacitance (TCC) within $\pm15\%$ of the 0.98NBBST–0.02NZN with the literature.

S.No	Composition	ε_r	TCC	Reference
1	$(0.90)[0.85\text{NBT–}0.15\text{BaCTi}_{1-y}\text{Zr}_y\text{O}_3]\text{–}0.10\text{NaNbO}_3$	2000	50 to 320 °C	49
2	$0.85[0.94\text{NBT–}0.06\text{BaTiO}_3]\text{–}0.15\text{KTaO}_3$	2070	0 to 282 °C	29
3	$(0.94)(\text{K}_{0.5}\text{La}_{0.5})_{0.1}\text{Ba}_{0.054}(\text{Bi}_{0.5}\text{Na}_{0.5})_{0.846}\text{Ti}_{0.95}(\text{Cr}_{0.5}\text{Ta}_{0.5})_{0.05}\text{O}_3\text{–}0.06\text{NaNbO}_3$	1800	58 to 338 °C	50
4	$0.98\text{Na}_{0.329}\text{Bi}_{0.329}\text{Ba}_{0.042}\text{Sr}_{0.30}\text{TiO}_3\text{–}0.02\text{Nd}(\text{Zn}_{2/3}\text{Nb}_{1/3})\text{O}_3$	2500	<RT to 324 °C	This work

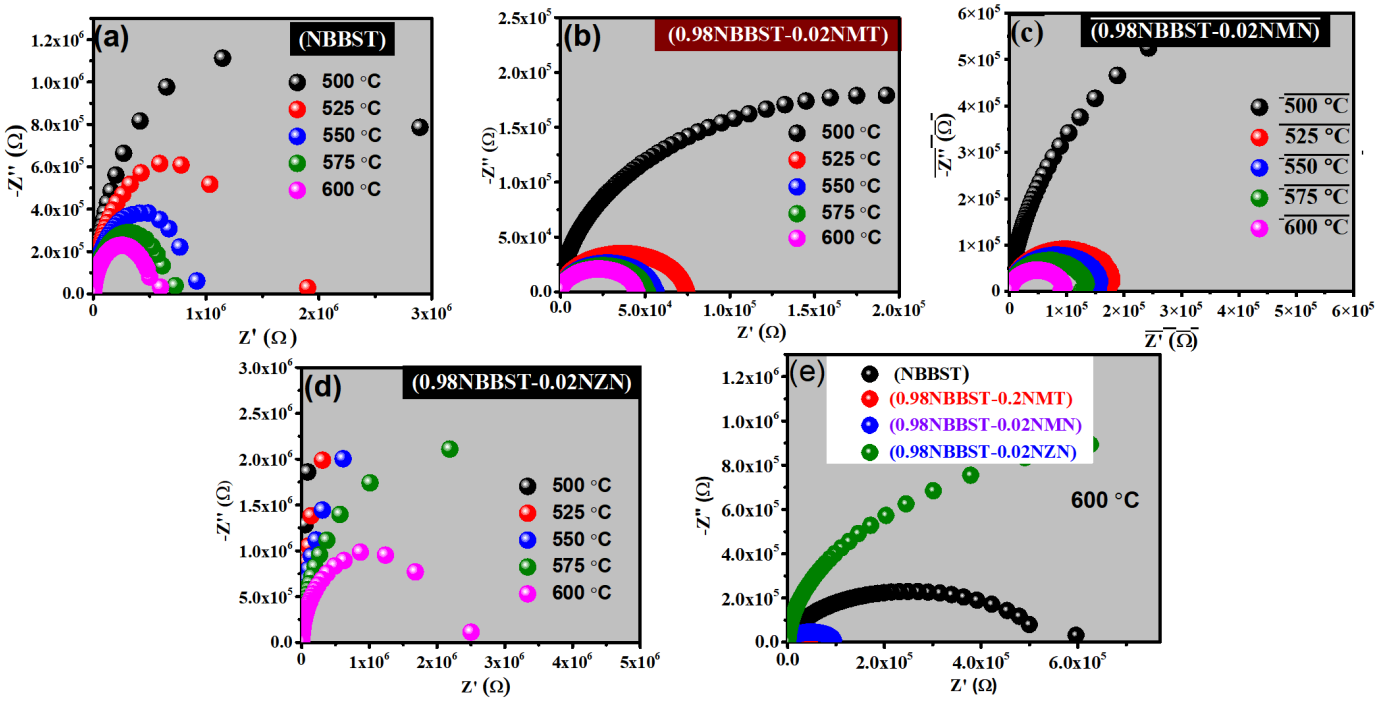

Figure 5. Nyquist ($-Z''$ vs Z') plots for (a) NBBST, (b) 0.98NBBST–0.02NMT, (c) 0.98NBBST–0.02NMN, (d) 0.98NBBST–0.02NZN ceramics measured in the frequency range 100 Hz–1 MHz and temperature range of $500 - - 600\,°C$. (e) Nyquist ($-Z''$ vs Z') plot of all compositions at $600\,°C$.

to 1 MHz. All compositions exhibit characteristic semicircular arcs whose diameters progressively decrease with increasing temperature, indicating enhanced electrical conductivity due to thermally activated charge carriers.

Typically, the observed Nyquist plots display initially arcs at temperature but becomes semicircles with increasing temperature. Only one arc or semicircle appeared at each temperature and for each composition, demonstrating that the resistance contribution is predominantly from grains only, consistent with impedance spectroscopy observations in other NBT-based perovskite ceramic systems [51, 52].

Importantly, the centers of these arcs or semicircles lie below the real axis, indicating non-ideal or non-Debye-type relaxation behavior. Such deviation from ideal Debye behavior is commonly observed across a wide range of functional oxide ceramics, including both ferroelectric perovskites and ferrite systems [53, 54]. This deviation from ideality is commonly associated with microstructural inhomogeneity, including grain size variations, random grain orientation, defect distributions, and internal stress–strain fields [55, 56]. Similar dielectric and impedance characterization approaches have been applied to related lead-free perovskite systems, including $BaTiO_3$-based ceramics modified with complex Bi-based oxides, further validating the analytical framework employed in the present study [50].

Further insight is provided in Figure 5(e), which compares the Nyquist plots of all compositions at $600\,°C$. Among them, the 0.98NBBST–0.02NZN ceramic exhibits the largest semicircular arc, implying the highest resistive behavior. In contrast, 0.98NBBST–0.02NMT and 0.98NBBST–0.02NMN ceramics display complete semicircles of smaller radii, while NBBST shows the smallest arc, corresponding to the lowest resistance. This comparative analysis clearly reveals that the 0.98NBBST–0.02NZN composition possesses superior resistivity at elevated temperatures, making it a promising candidate for high-temperature dielectric applications. The large semicircle of NZN-modified NBBST ceramics suggests maximum resistance arises from the unique $3d^{10}$ outer electronic configuration of Zn^{2+} cation, forming highly covalent chemical hybridizations with surrounding oxygen 2p orbitals, resulting in stabilizing the lattice and increasing the activation energy barrier for vacancy migration. Concurrently, the shift of lower-frequency apex shift (f_{max}) for the NZN arc signals that its large ionic radius generates strong localized structural distortions that act as deeper electrostatic trapping centers.

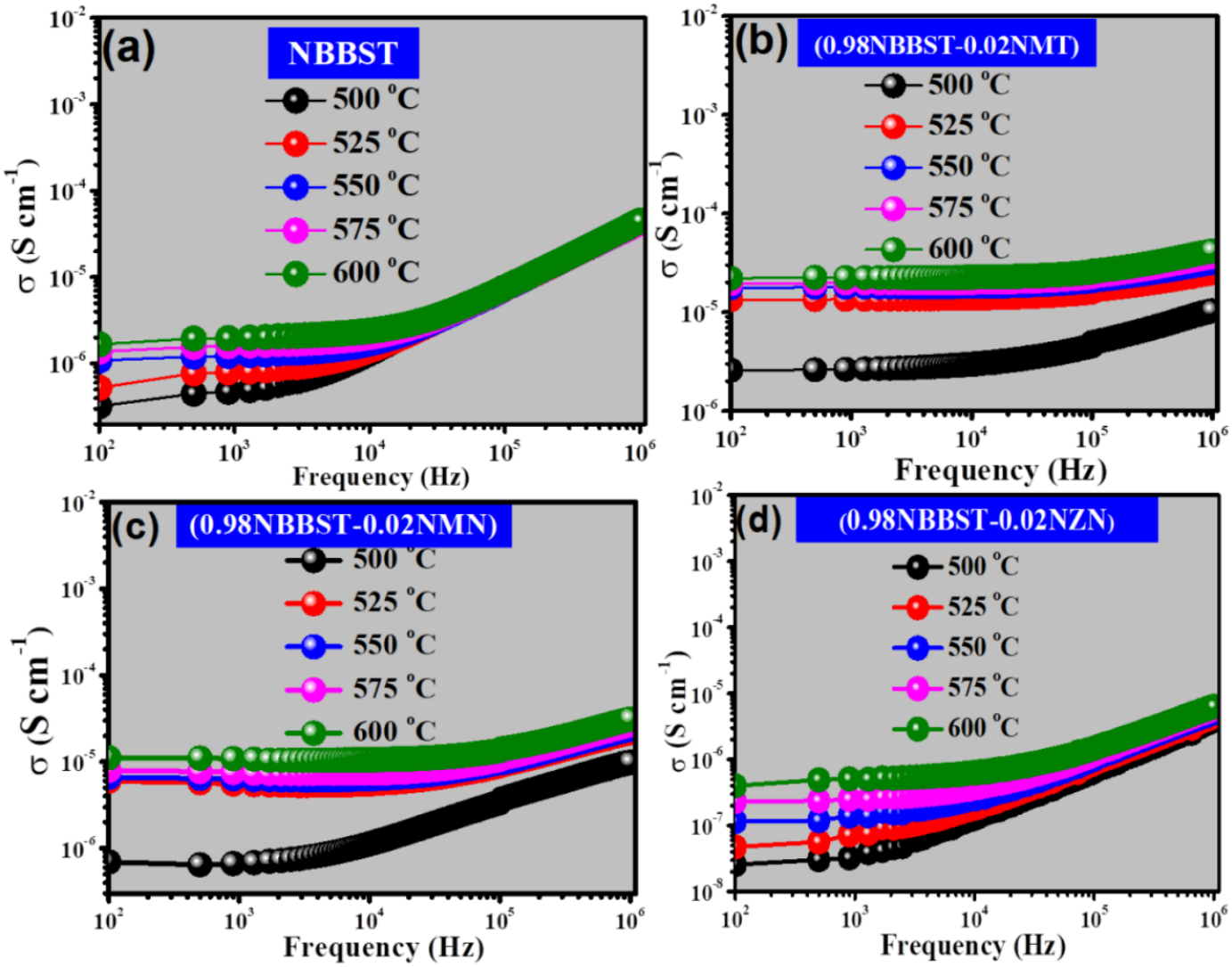

Figure 6. AC electrical conductivity (σ) vs temperature and frequency for (a) NBBST, (b) 0.98NBBST-0.02NMT, (c) 0.98NBBST-0.02NMN, and (d) 0.98NBBST-0.02NZN ceramics.

Furthermore, this reduction can be attributed to the substitution of Nb^{5+} as a donor dopant at the B-site, which helps to compensate for oxygen vacancies and effectively suppresses their formation, thereby reducing the overall conductivity of the material.

Another critical electrical property to be evaluated for dielectric materials is their electrical conductivity (σ), which arises from the movement of charge carriers within the material. Understanding this behavior is essential for assessing a material's suitability in electronic applications. Temperature-dependent conductivity measurements offer insights into the conduction behavior of thermally activated charge carriers, whereas frequency-dependent conductivity (σ_{ac}) studies help elucidate the mechanisms of charge transport—particularly hopping conduction [57].

In perovskite oxide ceramics, the conduction characteristics are intrinsically related to the mobility and density of charge carriers—particularly oxygen vacancies, whose migration and interaction with domain walls critically govern the overall electrical behavior [58]. In this study, the electrical conductivity (σ) of the NBBST, 0.98NBBST–0.02NMT, 0.98NBBST–0.02NMN, and 0.98NBBST–0.02NZN ceramics was determined using dielectric data, as shown in Figure 6, and calculated using the following relation [57]:

$$\sigma = \varepsilon_r \varepsilon_0 \omega \tan\delta \quad (1)$$

In Equation (1), ε_0 denotes the permittivity of free space, ε_r is the relative dielectric constant of the material, ω represents the angular frequency ($\omega = 2\pi f$), and $\tan\delta$ is the dielectric loss. The electrical conductivity of the ceramics generally increases with

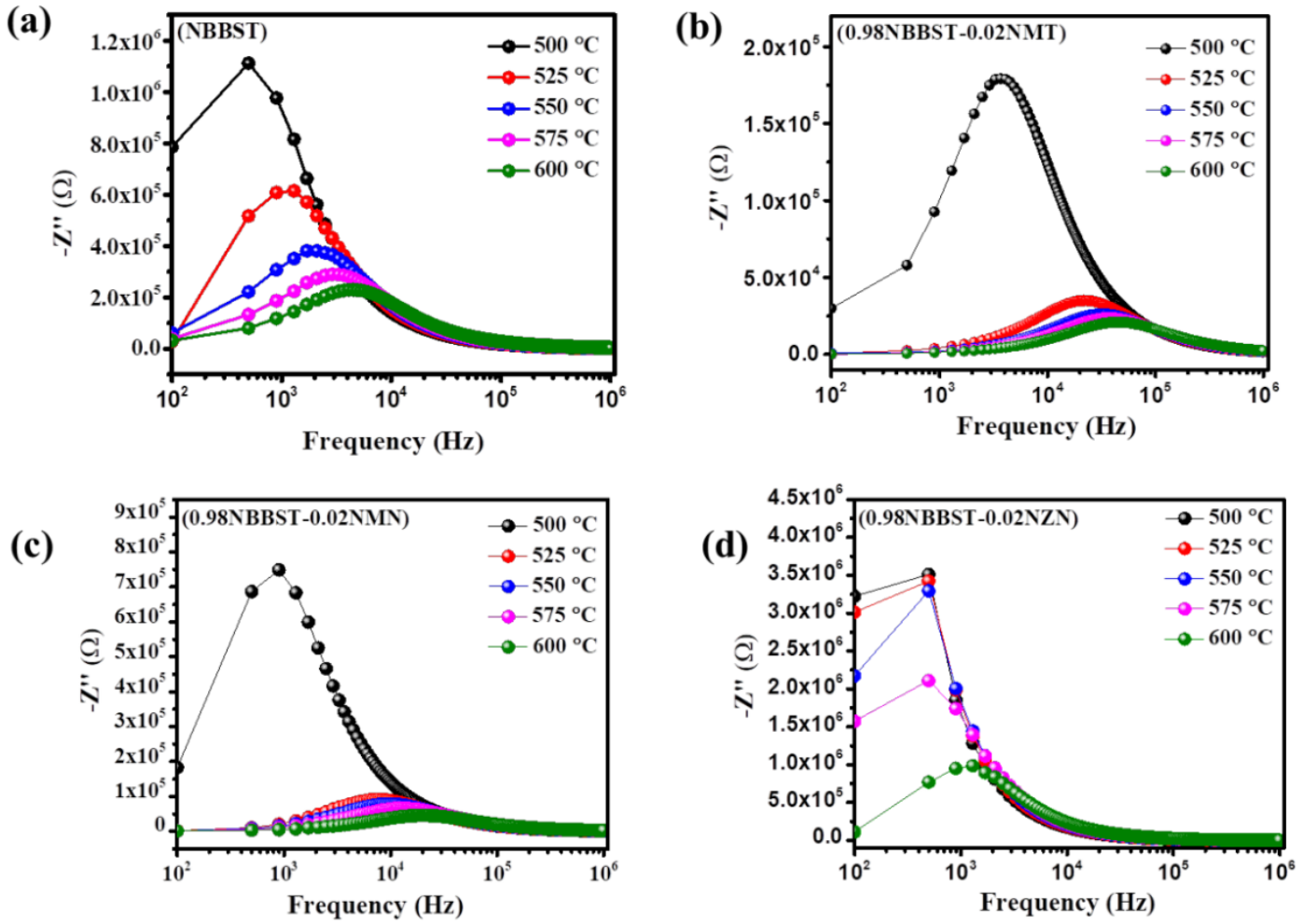

Figure 7. Frequency dependence of the imaginary part of impedance $(-Z'')$ at various temperatures $(500 - -600\,^{\circ}\mathrm{C})$ for NBBST, 0.98NBBST–0.02NMT, 0.98NBBST–0.02NMN, and 0.98NBBST–0.02NZN ceramics.

rising temperature, which can be attributed to the enhanced mobility of oxygen vacancies. These vacancies are often associated with the presence of highly polarizable Bi^{3+} ions and the relatively weak Bi–O bonds in BNT-based systems, which facilitate oxide ion conduction [60].

At lower temperatures, the electrical conductivity exhibits significant frequency dispersion, particularly in the low-frequency region. However, within this region, the conductivity tends to be nearly frequency-independent and is referred to as DC conductivity. As the temperature increases, a frequency-independent plateau becomes evident in the mid-frequency range, indicating the dominance of thermally activated conduction. In contrast, at high frequencies (above 1×10^5 Hz), a strong frequency dispersion is observed, and the conductivity curves for different temperatures tend to converge.

This temperature-dependent increase in conductivity reflects the negative temperature coefficient of resistance (NTCR) behavior typical of semiconducting oxide ceramics, as has been observed in various perovskite-based systems including both single-phase and compositionally complex compositions [59, 61]. The conduction mechanism in the frequency-independent region is governed by the hopping of charge carriers, such as ions, between adjacent vacant lattice sites. This process assumes that the carriers move through a lattice composed of equivalent potential wells. Additionally, the occurrence of charge hopping is characterized by a specific hopping frequency, beyond which carriers no longer respond effectively to the alternating field; this frequency-dependent conduction behavior has been documented in $Nd(Mg_{0.5}Ti_{0.5})O_3$-containing perovskite systems across a wide frequency range [62].

During the high-temperature processing of NBT-based ceramics, the volatility of Bi_2O_3 often leads to its loss, which in turn creates oxygen vacancies within the material [61]. These vacancies act

as charge carriers and contribute to increased electrical conductivity. In the present study, the DC electrical conductivity at 600 °C was found to be approximately 1.67×10^{-6} S/cm for NBBST. In contrast, a significantly lower electrical conductivity of approximately 3.98×10^{-7} S/cm was observed for the 0.98NBBST–0.02NZN ceramic at 600 °C.

Figure 7 presents the variation of the imaginary part of impedance ($-Z''$) as a function of frequency for all compositions at different temperatures. In all cases, $-Z''$ increases initially with frequency, reaches a maximum, and then decreases. As temperature increases, the peak of $-Z''$ shifts toward higher frequencies, suggesting a decrease in bulk resistance and a faster relaxation process. The convergence of the curves at high frequencies further confirms this behavior. Additionally, the broadening and asymmetry of the Z'' peaks with increasing temperature reflect the presence of multiple relaxation mechanisms. This is attributed to cationic disorder arising from the non-uniform distribution of A-site and B-site cations, which leads to a deviation from ideal Debye-type behavior. Among all compositions, the 0.98NBBST–0.02NZN ceramic exhibited higher $-Z''$ values and a slight shift of the peak to higher frequencies, indicating a higher resistive nature and slower relaxation dynamics compared to the other samples.

4 Conclusion

NBBST, 0.98NBBST–0.02NMT, 0.98NBBST–0.02NMN, and 0.98NBBST–0.02NZN ceramics were successfully synthesized using the conventional solid-state sintering method. The phase formation, microstructural features, dielectric behavior, and complex impedance characteristics of these compositions were systematically investigated. X-ray diffraction (XRD) analysis confirmed the formation of a single-phase perovskite structure for all samples. Scanning electron microscopy revealed a highly dense microstructure with suppressed grain growth in the doped compositions compared to the undoped NBBST. Among the investigated compositions, 0.98NBBST–0.02NZN demonstrated superior dielectric performance, exhibiting a high relative permittivity (ε_r) of $\sim$ 2500, low dielectric loss ($\tan\delta < 0.05$), reduced electrical conductivity $\sim 3.98 \times 10^{-7}$ S/cm measured at a frequency of 100 Hz and at 600 °C, and stable capacitance over a broad temperature range (below RT to 324 °C). Furthermore, impedance spectroscopy and Cole–Cole plot analysis indicated a higher resistance for the 0.98NBBST–0.02NZN ceramic at elevated temperatures, confirming its enhanced resistive nature. These findings suggest that the incorporation of suitable cationic dopants into the NBBST matrix significantly enhances its dielectric and thermal stability characteristics, making it a promising candidate for high-temperature capacitor applications.

Data Availability Statement

Data will be made available on request.

Funding

This work was supported by the National Research Program for Universities (NRPU) of the Higher Education Commission (HEC), Islamabad, Pakistan under Grant 20-17351/NRPU/R&D/HEC/2021.

Conflicts of Interest

The authors declare no conflicts of interest.

AI Use Statement

The authors declare that no generative AI was used in the preparation of this manuscript.

Ethical Approval and Consent to Participate

Not applicable.

References

[1] Takenaka, T., Maruyama, K., & Sakata, K. (1991). (Bi1/2Na1/2) TiO3-BaTiO3 system for lead-free piezoelectric ceramics. *Japanese journal of applied physics, 30*(9S), 2236. [CrossRef]

[2] Watson, J., & Castro, G. (2015). A review of high-temperature electronics technology and applications. *Journal of Materials Science: Materials in Electronics, 26*(12), 9226-9235. [CrossRef]

[3] Zeb, A., & Milne, S. J. (2015). High temperature dielectric ceramics: a review of temperature-stable high-permittivity perovskites. *Journal of Materials Science: Materials in Electronics, 26*(12), 9243-9255. [CrossRef]

[4] Dittmer, R., Jo, W., Damjanovic, D., & Rödel, J. (2011). Lead-free high-temperature dielectrics with wide operational range. *Journal of Applied Physics, 109*(3), 034107. [CrossRef]

[5] Dittmer, R., Anton, E. M., Jo, W., Simons, H., Daniels, J. E., Hoffman, M., Pokorny, J., Reaney, I. M., & Rödel, J. (2012). A high-temperature-capacitor dielectric based on $K_{0.5}Na_{0.5}NbO_3$-modified $Bi_{1/2}Na_{1/2}TiO_3$-$Bi_{1/2}K_{1/2}TiO_3$. *Journal of the*

American Ceramic Society, 95(11), 3519-3524. [CrossRef]

[6] Zeb, A., & Milne, S. J. (2013). Stability of high-temperature dielectric properties for (1-x)$Ba_{0.8}Ca_{0.2}TiO_3$-xBi($Mg_{0.5}Ti_{0.5}$)O_3 ceramics. *Journal of the American Ceramic Society, 96*(9), 2887-2892. [CrossRef]

[7] Zeb, A., Bai, Y., Button, T., & Milne, S. J. (2014). Temperature-stable relative permittivity from -70°C to 500°C in ($Ba_{0.8}Ca_{0.2}$)TiO_3-Bi($Mg_{0.5}Ti_{0.5}$)O_3-$NaNbO_3$ ceramics. *Journal of the American Ceramic Society, 97*(8), 2479-2483. [CrossRef]

[8] Zhang, Q., Li, Z., Li, F., & Xu, Z. (2011). Structural and dielectric properties of $BaTiO_3$-Bi($Mg_{0.5}Ti_{0.5}$)O_3 lead-free ceramics. *Journal of the American Ceramic Society, 94*(12), 4335-4339. [CrossRef]

[9] Raengthon, N., Sebastian, T., Cumming, D., Reaney, I. M., & Cann, D. P. (2012). BaTiO 3–Bi (Zn 1/2 Ti 1/2) O 3–BiScO 3 Ceramics for High-Temperature Capacitor Applications. *Journal of the American Ceramic Society, 95*(11), 3554-3561. [CrossRef]

[10] Zeb, A., & Milne, S. J. (2013). Dielectric properties of $Ba_{0.8}Ca_{0.2}TiO_3$-Bi($Mg_{0.5}Ti_{0.5}$)O_3-$NaNbO_3$ ceramics. *Journal of the American Ceramic Society, 96*(12), 3701-3703. [CrossRef]

[11] Li, H., Zhou, S., Zhao, J., Yan, T., Du, Y., Zhou, H., ... & Wang, D. (2023). Dielectric temperature stability and energy storage performance of NBT-based lead-free ceramics for Y9P capacitors. *Journal of Advanced Dielectrics, 13*(01), 2242007. [CrossRef]

[12] Xu, C., Lin, D., & Kwok, K. W. (2008). Structure, electrical properties and depolarization temperature of ($Bi_{0.5}Na_{0.5}$)TiO_3-$BaTiO_3$ lead-free piezoelectric ceramics. *Solid State Sciences, 10*(7), 934-940. [CrossRef]

[13] Zeb, A., & Milne, S. J. (2014). Low variation in relative permittivity over the temperature range 25-450°C for ceramics in the system (1-x)[$Ba_{0.8}Ca_{0.2}TiO_3$]-x[Bi($Zn_{0.5}Ti_{0.5}$)O_3]. *Journal of the European Ceramic Society, 34*(10), 1727-1732. [CrossRef]

[14] Kruea-In, C., Rujijanagul, G., Zhu, F. Y., & Milne, S. J. (2012). Relaxor behaviour of $K_{0.5}Bi_{0.5}TiO_3$-$BiScO_3$ ceramics. *Applied Physics Letters, 100*(20), 202904. [CrossRef]

[15] Jan, S. U., Zeb, A., & Milne, S. J. (2016). Dielectric ceramic with stable relative permittivity and low loss from -60°C to 300°C: A potential high temperature capacitor material. *Journal of the European Ceramic Society, 36*(11), 2713-2718. [CrossRef]

[16] Zeb, A., & Milne, S. J. (2014). Temperature-stable dielectric properties from -20°C to 430°C in the system $BaTiO_3$-Bi($Mg_{0.5}Z_{0.5}$)O_3. *Journal of the European Ceramic Society, 34*(13), 3159-3166. [CrossRef]

[17] Xu, Q., Lanagan, M. T., Luo, W., Zhang, L., Xie, J., Hao, H., Cao, M., Yao, Z., & Liu, H. (2016). Electrical properties and relaxation behavior of $Bi_{0.5}Na_{0.5}TiO_3$-$BaTiO_3$ ceramics modified with $NaNbO_3$. *Journal of the European Ceramic Society, 36*(10), 2469-2477. [CrossRef]

[18] Xu, Q., Song, Z., Tang, W., Hao, H., Zhang, L., Appiah, M., & Liu, H. (2015). Ultra-wide temperature stable dielectrics based on $Bi_{0.5}Na_{0.5}TiO_3$-$NaNbO_3$ system. *Journal of the American Ceramic Society, 98*(10), 3119-3126. [CrossRef]

[19] Höfling, M., Steiner, S., Hoang, A. P., Seo, I. T., & Frömling, T. (2018). Optimizing the defect chemistry of Na 1/2 Bi 1/2 TiO 3-based materials: paving the way for excellent high temperature capacitors. *Journal of Materials Chemistry C, 6*(17), 4769-4776. [CrossRef]

[20] Pu, Y., Yao, M., Liu, H., & Frömling, T. (2016). Phase transition behaviour, dielectric and ferroelectric properties of (1-x)($Bi_{0.5}Na_{0.5}$)TiO_3-x$Ba_{0.85}Ca_{0.15}Ti_{0.9}Zr_{0.1}O_3$ ceramics. *Journal of the European Ceramic Society, 36*(10), 2461-2468. [CrossRef]

[21] Jayakrishnan, A. R., Silva, J. P. B., Kamakshi, K., Dastan, D., Annapureddy, V., Pereira, M., & Sekhar, K. C. (2023). Are lead-free relaxor ferroelectric materials the most promising candidates for energy storage capacitors?. *Progress in Materials Science, 132*, 101046. [CrossRef]

[22] Dittmer, R., Jo, W., Rödel, J., Kalinin, S., & Balke, N. (2012). Nanoscale insight into lead-free BNT-BT-xKNN. *Advanced Functional Materials, 22*(20), 4208-4215. [CrossRef]

[23] Shi, J., Fan, H., Liu, X., Ma, Y., & Li, Q. (2015). Bi deficiencies induced high permittivity in lead-free BNBT-BST high-temperature dielectrics. *Journal of Alloys and Compounds, 627*, 463-467. [CrossRef]

[24] Liu, X., Fan, H., Shi, J., & Li, Q. (2015). Origin of anomalous giant dielectric performance in novel perovskite: $Bi_{0.5-x}$ La $_x$ $Na_{0.5-x}$ Li_x Ti_{1-y} M_y O_3 (M= Mg^{2+}, Ga^{3+}). *Scientific Reports, 5*(1), 12699. [CrossRef]

[25] Hiruma, Y., Nagata, H., & Takenaka, T. (2009). Thermal depoling process and piezoelectric properties of bismuth sodium titanate ceramics. *Journal of applied physics, 105*(8), 084112. [CrossRef]

[26] Kang, W., Li, Y., Zheng, Z., & Zhao, R. (2020). Enhanced dielectric and piezoelectric performance of (1-x)$Bi_{0.5}(Na_{0.78}K_{0.22})_{0.5}TiO_3$-x$BaTiO_3$ ceramics. *Ceramics International, 46*(11), 18089-18095. [CrossRef]

[27] Barick, B. K., Choudhary, R. N. P., & Pradhan, D. K. (2012). Phase transition and electrical properties of lanthanum-modified sodium bismuth titanate. *Materials Chemistry and Physics, 132*(3), 1007-1014. [CrossRef]

[28] Zhou, C., Liu, X., Li, W., & Yuan, C. (2009). Dielectric and piezoelectric properties of Bi0. 5Na0. 5TiO3–Bi0. 5K0. 5TiO3–BiCrO3 lead-free piezoelectric ceramics. *Journal of Alloys and Compounds, 478*(1-2), 381-385.

[CrossRef]

[29] Su, Y., Zhou, X., Xue, G., Luo, H., & Zhang, D. (2023). Temperature-stable $Na_{0.5}Bi_{0.5}TiO_3$-based ceramics with favourable low-temperature dielectric and energy storage property. *Journal of the American Ceramic Society, 106*(6), 3525-3536. [CrossRef]

[30] Cao, W., Li, W., Zhang, T., Sheng, J., Hou, Y., Feng, Y., Yu, Y., & Fei, W. (2015). High-energy storage density and efficiency of (1-x)[0.94NBT-0.06BT]-xST lead-free ceramics. *Energy Technology, 3*(12), 1198-1204. [CrossRef]

[31] Pan, Y., Dai, Z., Liu, C., Zhao, X., Yasui, S., Cong, Y., & Gu, S. (2024). High energy storage properties of $Nd(Mg_{2/3}Nb_{1/3})O_3$ modified $Bi_{0.5}Na_{0.5}TiO_3$ lead-free ceramics. *Journal of Materials Science, 59*(8), 3284-3296. [CrossRef]

[32] Li, W. Y., Zhou, D., Li, D., Guo, Y., Zhao, W. C., Pang, L. X., & Sun, S. K. (2023). High energy storage density in $Nd(Zn_{2/3}Nb_{1/3})O_3$-doped $BiFeO_3$-$BaTiO_3$ ceramics. *Advanced Electronic Materials, 9*(1), 2200930. [CrossRef]

[33] Sebastian, M. T. (2010). *Dielectric materials for wireless communication*. Elsevier. https://dl.acm.org/doi/abs/10.5555/1481425

[34] Hao, J., Bai, W., Li, W., & Zhai, J. (2012). Correlation between the microstructure and electrical properties in high-performance (Ba 0.85 Ca 0.15)(Zr 0.1 Ti 0.9) O 3 lead-free piezoelectric ceramics. *Journal of the American Ceramic Society, 95*(6), 1998-2006. [CrossRef]

[35] Yang, S., Liang, B., Liu, C., Liu, J., Fang, C., & Ai, Y. (2021). Microwave Sintering and Microwave Dielectric Properties of (1–x) Ca0. 61La0. 26TiO3-x Nd (Mg0. 5Ti0. 5) O3 Ceramics. *Materials, 14*(2), 438. [CrossRef]

[36] Ding, Y., Liu, J., Li, C., Bai, W., Wu, S., Zheng, P., ... & Zhai, J. (2021). High capacitive performance at moderate operating field in (Bi0. 5Na0. 5) TiO3-based dielectric ceramics via synergistic effect of site engineering strategy. *Chemical Engineering Journal, 426*, 130811. [CrossRef]

[37] Shannon, R. D. (1976). Revised effective ionic radii and systematic studies of interatomic distances in halides and chalcogenides. *Foundations of Crystallography, 32*(5), 751-767. [CrossRef]

[38] Hiruma, Y., Nagata, H., & Takenaka, T. (2008). Phase diagrams and electrical properties of $(Bi_{1/2}Na_{1/2})TiO_3$-based solid solutions. *Journal of Applied Physics, 104*(12), 124106. [CrossRef]

[39] Subohi, O., Bowen, C. R., Malik, M. M., & Kurchania, R. (2016). Dielectric spectroscopy and ferroelectric properties of magnesium-modified bismuth titanate ceramics. *Journal of Alloys and Compounds, 688*, 27-36. [CrossRef]

[40] Tu, C. S., Siny, I. G., & Schmidt, V. H. (1994). Sequence of dielectric anomalies and high-temperature relaxation behavior in $Bi_{1/2}Na_{1/2}TiO_3$. *Physical Review B, 49*(17), 11550-11559. [CrossRef]

[41] Bokov, A. A., & Ye, Z. G. (2006). Recent progress in relaxor ferroelectrics with perovskite structure. *Journal of materials science, 41*(1), 31-52. [CrossRef]

[42] Sakata, K., & Masuda, Y. (1974). Ferroelectric and antiferroelectric properties of $(Bi_{0.5}Na_{0.5})TiO_3$-$SrTiO_3$. *Ferroelectrics, 7*(5), 347-349. [CrossRef]

[43] Shannon, R. D. (1993). Dielectric polarizabilities of ions in oxides and fluorides. *Journal of Applied Physics, 73*(1), 348-366. [CrossRef]

[44] Jo, W., Schaab, S., Sapper, E., Schmitt, L. A., Kleebe, H. J., Bell, A. J., & Rödel, J. (2011). On the phase identity and its thermal evolution of lead free (Bi1/2Na1/2) TiO3-6 mol% BaTiO3. *Journal of Applied Physics, 110*(7). [CrossRef]

[45] Manan, A., Ullah, A., Khan, M. A., Ahmad, A. S., Iqbal, Y., Qazi, I., ... & Liu, H. (2022). Preparation, characterization, and improvement in the energy storage properties of Bi (Li0. 5Ta0. 5) O3 modified Na0. 5K0. 5NbO3 ceramic system. *Materials Research Bulletin, 145*, 111521. [CrossRef]

[46] Zhou, M., Liang, R., Zhou, Z., Yan, S., & Dong, X. (2018). Novel sodium niobate-based lead-free ceramics as new environment-friendly energy storage materials with high energy density, high power density, and excellent stability. *ACS Sustainable Chemistry & Engineering, 6*(10), 12755-12765. [CrossRef]

[47] Zeb, A., Jan, S. U., Bamiduro, F., Hall, D. A., & Milne, S. J. (2018). Temperature-stable dielectric ceramics based on $Na_{0.5}Bi_{0.5}TiO_3$. *Journal of the European Ceramic Society, 38*(4), 1548-1555. [CrossRef]

[48] Li, J., Li, F., Xu, Z., & Zhang, S. (2018). Multilayer lead-free ceramic capacitors with ultrahigh energy density and efficiency. *Advanced Materials, 30*(32), 1802155. [CrossRef]

[49] Qiao, Y., Li, J., Li, W., Li, M., Li, X., Ding, H., ... & Tan, X. (2024). Excellent high-temperature dielectric stability of BNT-based ceramics modified by NaNbO3. *Materials Today Communications, 38*, 108177. [CrossRef]

[50] Rehman, M. U., Manan, A., Ullah, A., Iqbal, Y., Khan, M. A., & Muhammad, R. (2023). Structural, dielectric and complex impedance analysis of Pb-free BaTiO3-Bi (Mg0. 5Ce0. 5) O3 ceramics. *Journal of Alloys and Compounds, 947*, 169575. [CrossRef]

[51] Tian, C., Tang, H., Liang, Y., Zhou, Y., Song, H., Yu, K., ... & Liu, G. (2025). Enhanced energy storage performance in SrTiO3-modified NBT-based lead-free ceramics via a stepwise strategy. *Journal of the American Ceramic Society, 108*(12), e70177. [CrossRef]

[52] Barick, B. K., Choudhary, R. N. P., & Pradhan, D. K. (2013). Dielectric and impedance spectroscopy of zirconium modified (Na0. 5Bi0. 5) TiO3 ceramics. *Ceramics International, 39*(5), 5695-5704. [CrossRef]

[53] Hcini, S., Omri, A., Boudard, M., Bouazizi, M. L., Dhahri, A., & Touileb, K. (2018). Microstructural,

magnetic and electrical properties of Zn0. 4M0. 3Co0. 3Fe2O4 (M= Ni and Cu) ferrites synthesized by sol–gel method. *Journal of Materials Science: Materials in Electronics, 29*(8), 6879-6891. [CrossRef]

[54] Zhao, P., Fang, Z., Zhang, X., Chen, J., Shen, Y., Zhang, X., ... & Tang, B. (2021). Aliovalent doping engineering for A-and B-sites with multiple regulatory mechanisms: a strategy to improve energy storage properties of Sr0. 7Bi0. 2TiO3-based lead-free relaxor ferroelectric ceramics. *ACS applied materials & interfaces, 13*(21), 24833-24855. [CrossRef]

[55] Sen, S., Choudhary, R. N. P., Tarafdar, A., & Pramanik, P. (2006). Impedance spectroscopy study of strontium modified lead zirconate titanate ceramics. *Journal of applied physics, 99*(12). [CrossRef]

[56] Sinclair, D. C., & West, A. R. (1989). Impedance and modulus spectroscopy of semiconducting BaTiO3 showing positive temperature coefficient of resistance. *Journal of Applied Physics, 66*(8), 3850-3856. [CrossRef]

[57] Sareecha, N., Shah, W. A., Mirza, M. L., Maqsood, A., & Awan, M. S. (2018). Electrical investigations of Bi-doped BaTiO3 ceramics as a function of temperature. *Physica B: Condensed Matter, 530*, 283-289. [CrossRef]

[58] Li, W., Chen, A., Lu, X., & Zhu, J. (2005). Collective domain-wall pinning of oxygen vacancies. *Journal of Applied Physics, 98*(2), 024109. [CrossRef]

[59] Mohanty, B., Bhattacharjee, S., Nayak, N. C., Parida, R. K., & Parida, B. N. (2021). Dielectric, magnetic and optical study of La-doped BFO-BST ceramic for multifunctional applications. *Materials Science in Semiconductor Processing, 128*, 105720. [CrossRef]

[60] Li, M., Pietrowski, M. J., De Souza, R. A., Zhang, H., Reaney, I. M., Cook, S. N., ... & Sinclair, D. C. (2014). A family of oxide ion conductors based on the ferroelectric perovskite Na0. 5Bi0. 5TiO3. *Nature materials, 13*(1), 31-35. [CrossRef]

[61] Zhao, N., Zheng, X., Huang, F., Wang, L., Qian, X., Li, Z., ... & Fan, H. (2024). Enhanced energy storage properties of Sm (Mg0. 5Ti0. 5) O3 modified (Bi0. 5Na0. 5) 0.7 Sr0. 3TiO3 relaxor ferroelectric ceramics. *Ceramics International, 50*(5), 8325-8331. [CrossRef]

[62] Kim, J. B., Yoon, K. H., & Cho, Y. S. (2003). Compositional Dependence of Microwave Dielectric Properties in (1-x)(Na1/2Nd1/2) TiO3-xNd (Mg1/2Ti1/2) O3 Ceramics. *Journal of the American Ceramic Society, 86*(7), 1159-1161. [CrossRef]

Aamir Jalil received the M.S. degree in Physics, from the Department of Physics and Materials Science, University of Science & Technology Bannu, Khyber Pakhtunkhwa, Pakistan in 2024. (Email: aamirjalil390@gmail.com)

Shah Faisal received the MS degree in Chemistry from the department of Chemical Sciences, University of Science & Technology Bannu, Khyber Pakhtunkhwa, Pakistan in 2024. His research focus on processing of dielectric materials for telecommunication as well as energy storage capacitors. (Email: sf8443@gmail.com)

Abdul Manan received the PhD. degree in Physics, from the department of Physics, University of Peshawar Pakistan in 2011. He did his Postdoctorate from School of Materials Science and Engineering, Wuhan University Technology, China and 2017 as well as from the Materials Research Institute, the Pennsylvania State University, USA in 2023. His research focus on the designing of dielectric materials for resonators, energy storage capacitors applications etc. He is the author of more than 100 research articles. He is currently working as an Associate Professor at the Department of Physics and Materials Science, University of Science & Technology Bannu, Pakistan (Email: drmanan2@ustb.ed.pk, drmanan82@yahoo.com)

Imran Ullah received the BS degree in Physics, from the Department of Physics and Materials Science, University of Science & Technology Bannu, Khyber Pakhtunkhwa, Pakistan in 2024. (Email: iu2393961@gmail.com)

Safeer Ahmad received the PhD. degree in Physics, from the department of Physics, University of Peshawar Pakistan in 2016. He is director, center for Materials Science, Islamia college Peshawar. He is the author of more than 50 research articles. He is currently working as Director, center for Materials Science, Islamia College Peshawar, Pakistan. (Email: arbab.safeer@icp.edu.pk)

Ameer Ullah received the MS degree in Physics from the department of Physics and materials Science, University of Science & Technology Bannu, Khyber Pakhtunkhwa in 2024. (Email: ameerullah59@gmail.com)